

## Magnetic properties of vanadium oxide nanotubes and nanolayers

S. V. Demishev,<sup>1,\*</sup> A. L. Chernobrovkin,<sup>1,2</sup> V. V. Glushkov,<sup>1</sup> A. V. Grigorieva,<sup>3</sup> E. A. Goodilin,<sup>3</sup> H. Ohta,<sup>4</sup> S. Okubo,<sup>4</sup> M. Fujisawa,<sup>4</sup> T. Sakurai,<sup>5</sup> N. E. Sluchanko,<sup>1</sup> N. A. Samarin,<sup>1</sup> and A. V. Semeno<sup>1</sup>

<sup>1</sup>*A.M. Prokhorov General Physics Institute of RAS, 38 Vavilov Street, Moscow 119991, Russia*

<sup>2</sup>*Institute of Biomedical Chemistry, Russian Academy of Medical Sciences, 10 Pogodinskaya Street, Moscow 119121, Russia*

<sup>3</sup>*M.V. Lomonosov Moscow State University, Materials Science Department, Vorob'evy Gory, Moscow 119991, Russia*

<sup>4</sup>*Molecular Photoscience Research Center, Kobe University, 1-1 Rokkodai, Nada, Kobe 657-8501, Japan*

<sup>5</sup>*Center for Supports to Research and Education Activities, Kobe University, Kobe 657-8501, Japan*

(Received 26 April 2011; revised manuscript received 8 July 2011; published 20 September 2011)

We report results of magnetic measurements of VO<sub>x</sub> nanolayers (stacks of four to eight distorted layers of vanadium oxide separated by an organic template) obtained at the early stages of a hydrothermal synthesis of VO<sub>x</sub> nanotubes (VO<sub>x</sub> NTs), and VO<sub>x</sub> NTs themselves, which are the product of scrolling of VO<sub>x</sub> nanolayers (VO<sub>x</sub> NLs). Static and dynamic magnetic properties of VO<sub>x</sub> NLs and VO<sub>x</sub> NTs have been studied by means of a high-frequency (60 GHz) ESR and SQUID magnetometry in a temperature range 1.8–300 K. The temperature dependence of the magnetic susceptibility  $\chi$  of the V<sup>4+</sup> quasifree spins in VO<sub>x</sub> NTs and VO<sub>x</sub> NLs shows a transition from the Curie-Weiss laws with close paramagnetic temperatures  $\Theta_{\text{AFM}} = -25$  K (VO<sub>x</sub> NTs) and  $\Theta_{\text{AFM}} = -19$  K (VO<sub>x</sub> NLs) to the low-temperature power law  $\chi \propto 1/T^\xi$  with  $\xi = 0.75$  (VO<sub>x</sub> NTs) and  $\xi = 0.85$  (VO<sub>x</sub> NLs). The observed  $\chi(T)$  dependence for quasifree spins was adequately described within an analytical model of an antiferromagnetic system with a disorder-driven quantum critical behavior. Comparison of static and dynamic susceptibilities reveals that the total magnetic susceptibility in VO<sub>x</sub> NLs and VO<sub>x</sub>-NTs consists of several contributions. Apart from the oscillating susceptibility, there is a nonoscillating background, likely, consisting of the Van Vleck-type and Pauli-type terms. In the case of VO<sub>x</sub> NTs, a correlated change of the Curie constant for the nondimerized V<sup>4+</sup> quasifree spins and a variation of the background are observed: the decrease in temperature in the interval  $70 \text{ K} < T < 120 \text{ K}$  induces 1.8-fold growth of the Curie constant followed by a nonoscillating background decrease along with a change of its sign. The estimated concentration of magnetic sites indicates that a characteristic feature of VO<sub>x</sub> NLs and VO<sub>x</sub> NTs is a discrepancy between the maximal possible concentration of V<sup>4+</sup> magnetic ions that is allowed by a chemical composition, and a concentration of the localized magnetic moments. The number of electrons in the V<sup>4+</sup> state is always less than the total electron concentration, and the concentration of the “excessive” electrons may vary in the range 0.11–0.46 per vanadium site. At the same time, the concentration of V<sup>4+</sup>-V<sup>4+</sup> antiferromagnetic dimers in VO<sub>x</sub> NTs is rather high and reaches 49% of all vanadium sites. The effects of scrolling and Mott-Hubbard-type models of unusual magnetism in the VO<sub>x</sub> nanomaterials are discussed.

DOI: [10.1103/PhysRevB.84.094426](https://doi.org/10.1103/PhysRevB.84.094426)

PACS number(s): 81.07.De, 76.30.Fc, 75.47.Lx, 75.50.Tt

### I. INTRODUCTION

Analyzing the magnetic properties of various vanadium oxide (VO<sub>x</sub>) based nanomaterials has recently attracted much attention.<sup>1–8</sup> The interest in this field of research was stimulated by the observation of the room-temperature ferromagnetism in doped VO<sub>x</sub> multiwall nanotubes (VO<sub>x</sub> NTs).<sup>1</sup> However, even pure (undoped) VO<sub>x</sub> NTs, which are supposed to be antiferromagnets,<sup>2</sup> demonstrate a strong departure from the Curie-Weiss law at temperatures  $T > 100$  K due to the presence of antiferromagnetic (AFM) dimers formed by V<sup>4+</sup>  $S = 1/2$  magnetic ions.<sup>2</sup> Some features of magnetization and NMR spectra in VO<sub>x</sub> NTs have been assigned to the trimers or other complex V<sup>4+</sup>  $S = 1/2$  spin clusters.<sup>2</sup> Further development of the “clusterization” idea has led to a discussion of the disorder driven quantum critical phenomena in VO<sub>x</sub>-NTs.<sup>6</sup> According to Ref. 6, the ground state for VO<sub>x</sub> NTs is expected to be the Griffiths phase,<sup>9–11</sup> which is characterized by dispersion of the exchange constants and the V<sup>4+</sup> magnetic subsystem decomposition into coupled spin clusters of a nanometer size.<sup>12,13</sup>

Another interesting feature of the magnetic properties of VO<sub>x</sub> NTs is a so-called FM-AFM crossover<sup>7</sup> consisting of a

transition at  $T \sim 100$  K from the ferromagnetic (FM) Curie-Weiss temperature dependence of dynamic susceptibility to an antiferromagnetic one with a temperature decrease. This effect is accompanied by a noticeable increase of Curie constant at low temperatures, which may be a consequence of a change in the V<sup>4+</sup> magnetic ion concentration.<sup>7</sup>

However, it is not easy to find concentrations of various spin species in the VO<sub>x</sub> NTs. The estimates following from the static magnetization reported in Ref. 2 demonstrate a discrepancy at high and low temperatures, where the number of spins at low temperatures is less than at high temperatures. At the same time dynamic data suggest opposite behavior.<sup>7</sup>

Resolving this controversial situation requires information about various magnetic contributions, which form magnetic response of the VO<sub>x</sub> nanomaterials, in particular VO<sub>x</sub> NTs. A solution of this problem was attempted in Ref. 14 but the applied procedure of separation of various terms was not well justified and was a kind of *ad hoc* assumption.

The aforementioned difficulties on one hand reflect poor understanding of the fundamental magnetization structure in various VO<sub>x</sub> nanomaterials. On the other hand, the clarification may be achieved if the unusual magnetic properties of VO<sub>x</sub> NTs will be considered in a wider context. Indeed, some of the

vanadium oxide nanomaterials could be considered as belonging to the same class, where  $\text{VO}_x$  planes or  $\text{VO}_x$  corrugated layers consist of the  $\text{V}^{4+}$  magnetic and  $\text{V}^{5+}$  nonmagnetic ions<sup>2</sup> that define properties of magnetic subsystems. In addition, the considered  $\text{VO}_x$  nanomaterials are prepared by the same method of the hydrothermal treatment of vanadium pentoxide  $\text{V}_2\text{O}_5$  in the presence of various organic compounds such as long chain amines and alcohols.<sup>1-8,15-17</sup> This technique provides morphologically different samples with common structural fragments by direct varying the synthesis conditions (such as time of hydrothermal treatment, the  $p\text{H}$  of the medium, etc.<sup>1-8,15-17</sup>). As long as this class of materials may have common structural motive, it may be rewarding to analyze comparatively the physical properties of  $\text{VO}_x$  nanomaterials, for example layered and scrolled amine-templated vanadium oxides,<sup>15</sup> in order to achieve better understanding of their anomalous magnetism.

Following this line, in the present work, we focus on the analysis of magnetic properties of the vanadium oxide nanolayers ( $\text{VO}_x$  NLs) and  $\text{VO}_x$  nanotubes. The  $\text{VO}_x$  NLs are the product obtained at early stages of the  $\text{VO}_x$  NTs hydrothermal synthesis, which precedes a formation of nanotubes. Structurally, the individual nanoparticle in the  $\text{VO}_x$ -NLs sample is a stack of four to eight distorted layers of vanadium oxide separated by an organic template. An increasing synthesis time leads to the scrolling of such layers with a multiwall nanotube formation. An essential dissimilarity in magnetic properties of  $\text{VO}_x$  NLs and  $\text{VO}_x$  NTs reported in Ref. 7 consists of the absence of the FM-AFM crossover in nanolayers. As long as  $\text{VO}_x$  NLs and  $\text{VO}_x$  NTs are closest analogs among vanadium oxide nanomaterials, their comparative study is important for correct determination of the magnetization structure and obtaining correct values of various spin states. Moreover, such comparison may elucidate the nature of the crossover effect as well as shed light on the genesis of the quantum critical phenomena. In the present work for the analysis of the temperature dependence of the susceptibility, a recently developed model of disorder driven quantum critical phenomena,<sup>12,13</sup> which enables describing magnetic properties at an arbitrary temperature, will be used. This approach to the data analysis allows improving the reliability of the calculated Curie constants.

From the structural point of view the main difference between  $\text{VO}_x$  NLs and  $\text{VO}_x$  NTs is the scrolling of the  $\text{VO}_x$  planes. Although the structural effect of scrolling has been examined in detail,<sup>18</sup> to our best knowledge the influence of scrolling on the magnetic properties including the dimers problem and FM-AFM crossover<sup>7</sup> has not been analyzed up to now. In the present work we are going to try to fill this gap.

The paper is organized as follows. After providing information about samples synthesis, structure, and chemical composition together with the details of the methods used (Sec. II) the electron-spin resonance (ESR) data will be briefly discussed (Sec. III). Section IV describes the procedure of the separation of various contributions to total susceptibility and display obtained results for  $\text{VO}_x$  NLs and  $\text{VO}_x$  NTs. This part forms the basis for the discussion of the low-temperature anomaly, determination of Curie constants (Sec. V), and for calculation of the concentrations of various spin states and contains a different interpretation of the FM-AFM crossover

effect (Sec. VI). An unexpected result of quantitative analysis of the static and dynamic magnetic properties is that the number of electrons in  $\text{V}^{4+}$  states is always less than the total electron concentration, which brings to the agenda modification of Mott-Hubbard-type models initially suggested in (Ref. 1) for the explanation of the anomalous magnetism of the vanadium oxide nanotubes. In conclusion, the effect of scrolling on the magnetic properties of the  $\text{VO}_x$  nanomaterials is discussed.

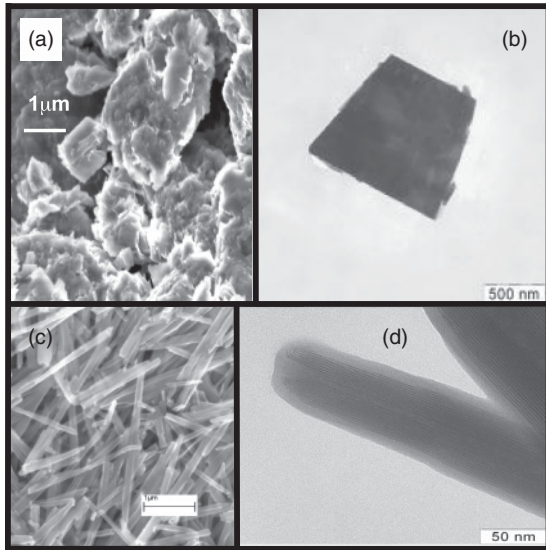
## II. EXPERIMENTAL DETAILS

The sample preparation technique was similar to that described in Refs. 16 and 17.  $\text{VO}_x$  NLs and  $\text{VO}_x$  NTs were synthesized by a hydrothermal treatment of orthorhombic vanadium pentoxide (Sigma Aldrich).<sup>16</sup> Crystalline 1-hexadecylamine (HDA,  $\text{C}_{16}\text{H}_{33}\text{NH}_2$ , Sigma Aldrich) was used as a molecular template for obtaining layered  $\text{VO}_x$  nanomaterials, discussed below. After a homogenization step, near the 2-h hydrothermal treatment at  $\sim 180^\circ\text{C}$  resulted in  $\text{VO}_x$ -NL formation with the template molecules intercalated between  $\text{VO}_x$  distorted planes. Further extension of the synthesis time up to 160 h resulted in an increasing yield of nanotubular structures because of self-scrolling of  $\text{VO}_x$ -NLs into  $\text{VO}_x$  NTs.

The x-ray analysis data show that the unit cell in the  $\text{VO}_x$  plane in nanolayers is close to a square cell, contains seven vanadium atoms, and has the cell parameter of 6.13(1) Å, whereas the distance between the  $\text{VO}_x$  layers is near 33 Å. The description of the  $\text{VO}_x$  NTs structure is a more complex problem due to bending of the  $\text{VO}_x$  layers under scrolling. However, it is possible to conclude from our data that, if fine bending effects are neglected, both the size of the quasiunit cell in the scrolled  $\text{VO}_x$  plane and the interlayer distance in  $\text{VO}_x$  NTs almost coincide with the corresponding structure parameters for  $\text{VO}_x$  NLs. These facts reasonably agree with the structural results reported previously.<sup>18</sup>

The microstructure of  $\text{VO}_x$  NLs and  $\text{VO}_x$  NTs was examined by a scanning electron microscopy (SEM). The examples of SEM images are presented in Fig. 1. It can be seen that the structure of both  $\text{VO}_x$  NLs and  $\text{VO}_x$  NTs is characterized by a built-in disorder. The  $\text{VO}_x$  layers are corrugated in  $\text{VO}_x$  NLs [Figs. 1(a) and 1(b)] and are not closed concentrically in  $\text{VO}_x$  NTs [Figs. 1(c) and 1(d)]. Additionally, the open ends and bending of the nanotubes may serve as other sources of structural defects [Figs. 1(c) and 1(d)]. The estimated nanotube diameter was found to be of about 50–100 nm and the length was in the range 2–10  $\mu\text{m}$ .

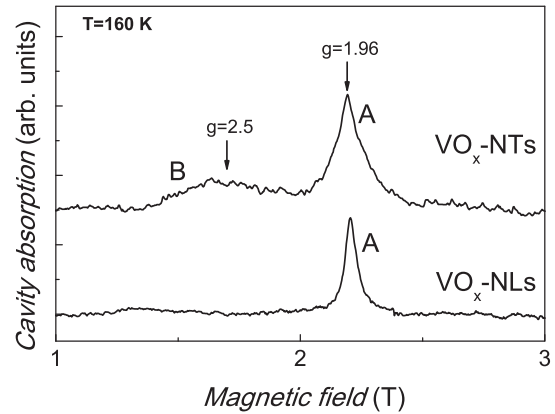
The x-ray photoelectron spectroscopy and chemical analysis data have provided the following chemical compositions:  $\text{VO}_{2.11}(\text{C}_{16}\text{H}_{33}\text{NH}_2)_{0.41}$  and  $\text{VO}_{2.17}(\text{C}_{16}\text{H}_{33}\text{NH}_2)_{0.55}$  for  $\text{VO}_x$  NTs and  $\text{VO}_x$  NLs, respectively. This corresponds to the average vanadium charge  $\zeta = +4.22$  in  $\text{VO}_x$  NTs and  $\zeta = +4.34$  in  $\text{VO}_x$  NLs. The template content in these nanomaterials matches roughly the “ideal” composition, in which there is one template molecule in the interlayer space per two  $\text{VO}_x$  units as it was proposed in some models recently.<sup>1,19</sup> From this point of view, a slight deviation from the model structure<sup>1,19</sup> in  $\text{VO}_x$  NTs and  $\text{VO}_x$  NLs would be attributed to their imperfect structure (see Fig. 1).


 FIG. 1. SEM images of (a),(b)  $\text{VO}_x$  NLs and (c),(d)  $\text{VO}_x$  NTs.

The static magnetization measurements were carried out in the temperature range 1.8–300 K in magnetic fields up to 5 T by means of a SQUID magnetometer (Quantum Design). Special attention was paid to subtraction of the magnetic response of the measuring cell. The accuracy of the sample mass measuring by the balance used was better than 0.001 mg. The dynamic magnetic response was deduced from the electron spin resonance (ESR) measurements, which were performed at a frequency 60 GHz in magnetic fields up to 7 T for temperatures 4.2–250 K using an original cavity magneto-optical spectrometer.<sup>20</sup> The transmission of the cylindrical cavity operating at the  $\text{TE}_{011}$  mode was measured as a magnetic-field function at each particular temperature; the accuracy of the temperature stabilization was better than 0.01 K. The cavity was connected to the waveguide line in a reflection geometry and the investigated sample was placed in the maximum of the oscillating magnetic field at the cavity bottom. The quality factor of the cavity loaded with the  $\text{VO}_x$  nanomaterial was about  $10^4$ .

### III. ELECTRON SPIN RESONANCE

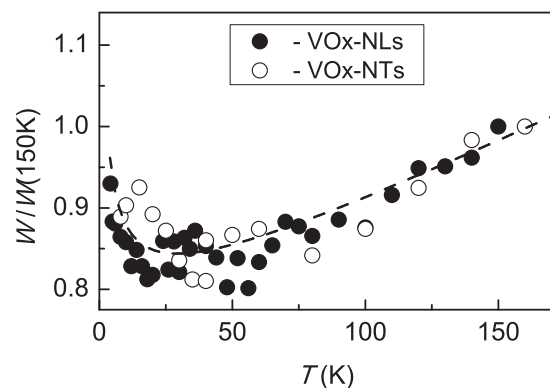
The ESR spectra for  $\text{VO}_x$  NTs were examined in detail in Refs. 6 and 7. It was established that in this material there are two absorption lines A and B (Fig. 2), one (A) with the temperature-independent  $g$  factor  $g = 1.96 \pm 0.02$ . This value is known to correspond to the angle averaged  $g$  factor for  $\text{V}^{4+}$   $S = 1/2$  ions.<sup>3,4</sup> The line B with the  $g$  factor  $g = 2.5 \pm 0.1$  originates from the magnetic resonance on the excited triplet state of  $\text{V}^{4+}$ - $\text{V}^{4+}$  AF dimers.<sup>6,7</sup> The integrated intensity of this line can be well described by the standard expression for the susceptibility of AFM dimers  $\chi(T) = C_d/T[3 + \exp(\Delta/k_B T)]$ , where  $\Delta$  denotes the spin gap and  $C_d$  is the Curie constant for dimers. The value of the spin gap reported in Refs. 6 and 7 is  $\Delta = 720 \pm 20$  K and agrees well with the independent estimates obtained in Refs. 1 and 2. It is worth noting that the observed  $g$  factor for the dimers is noticeably renormalized with respect to the


 FIG. 2. ESR spectra at temperature  $T = 160$  K for the  $\text{VO}_x$  NTs (upper) and  $\text{VO}_x$  NLs (lower). Line A corresponds to  $\text{V}^{4+}$  quasifree spins and line B originates from the  $\text{V}^{4+}$ - $\text{V}^{4+}$  antiferromagnetic dimers.

value characteristic to  $\text{V}^{4+}$  quasifree spins. The reasons for this behavior have not been discussed up to now and this problem will be addressed at the end of the paper (Sec. VII).

The ESR spectrum for  $\text{VO}_x$  NLs is simpler and consists of a single line corresponding to  $\text{V}^{4+}$  quasifree spins with the same temperature-independent  $g$  factor as in the case of  $\text{VO}_x$  NTs (Fig. 2). However, the resonance A linewidth  $W$  for  $\text{VO}_x$  NTs is different from that for  $\text{VO}_x$  NLs. Assuming the Lorentzian line shape, the half width at half maximum equals  $W = 0.16$  T at  $T = 150$  K for nanotubes whereas for nanolayers, the linewidth at the same temperature is three times smaller,  $W = 0.054$  T. At the same time the normalized temperature dependence  $W(T)/W(150 \text{ K})$  almost coincides for  $\text{VO}_x$  NLs and  $\text{VO}_x$  NTs (Fig. 3). The  $W(T)$  curve goes down by  $\sim 20\%$  with decreasing temperature, passes through a minimum at  $T \sim 30$ – $50$  K, and then starts to increase (Fig. 3). The universal normalized temperature dependence of the linewidth indicates that the physical mechanisms of spin relaxation may be very close in  $\text{VO}_x$  NLs and  $\text{VO}_x$  NTs, but the magnitude of spin fluctuations and (or) disorder rate are higher for nanotubes as suggested by absolute values of  $W$ .

The data for the ESR line integrated intensities are presented in Figs. 4 and 5 for  $\text{VO}_x$  NLs and  $\text{VO}_x$  NTs, respectively. The measured field dependences of magnetization  $M(H)$  show the


 FIG. 3. Reduced linewidths for the ESR lines A and B in  $\text{VO}_x$  NTs.

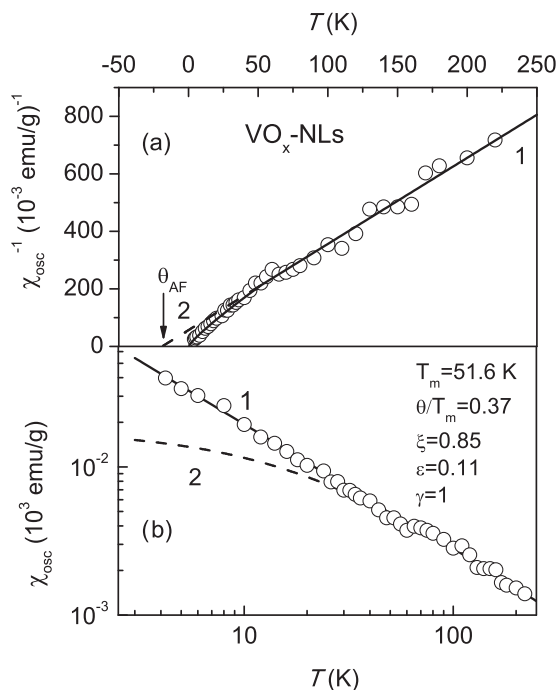


FIG. 4. Temperature dependence of the oscillating part of magnetic susceptibility for  $\text{VO}_x$  NLS (a) in the Curie-Weiss coordinates and (b) in the logarithmic coordinates. Circles denote the experiment results, curves 1 are the quantum critical model fit, and curves 2 correspond to the Curie-Weiss fit (see text for details). The paramagnetic temperature is marked by an arrow.

nonlinearity of the magnetic response at the ESR resonant field for 60 GHz does not exceed  $\sim 3\%$  at  $T > 4.2$  K. Thus within a reasonable accuracy, the integrated intensity  $I$  in our case is proportional to the part of the spin susceptibility  $\chi_{\text{osc}}$ , which contributes to magnetic oscillations,  $I(T) \propto \chi_{\text{osc}}(T)$ . The procedure of obtaining the absolute scale for  $\chi_{\text{osc}}$  is explained in the next section. Here the functional dependences  $\chi_{\text{osc}}(T)$  are considered.

For  $\text{VO}_x$  NLS the susceptibility  $\chi_{\text{osc}}(T)$  follows the Curie-Weiss law  $\chi_{\text{osc}}(T) = C/(T - \Theta)$  at  $T > 50$  K, which can be seen from the plot in coordinates  $\chi_{\text{osc}}^{-1} = f(T)$  [Fig. 4(a)]. The sign of the paramagnetic temperature  $\Theta$  is negative, which corresponds to antiferromagnetic interaction, and the data in Fig. 4 give  $\Theta_{\text{AFM}} = -(19 \pm 1)$  K for  $\text{VO}_x$  NLS. Below  $T \sim 50$  K, a deviation from the Curie-Weiss law is observed at low temperatures; the curve  $\chi_{\text{osc}}(T)$  is described by the power law  $\chi_{\text{osc}}(T) \propto 1/T^\xi$  with  $\xi \sim 0.8$  [see Fig. 4(b)].

The temperature dependence of  $\chi_{\text{osc}}$  in the case of  $\text{VO}_x$  NTs for line A is essentially different. In the range  $T > T_C \sim 70$  K, the oscillating susceptibility within experimental accuracy may be approximated by the Curie-Weiss law for a ferromagnet with  $\Theta_{\text{FM}} = (32 \pm 2)$  K [Fig. 5(a)]. For  $T < T_C$ , the slope of the linear section in coordinates  $\chi_{\text{osc}}^{-1} = f(T)$  decreases suggesting a noticeable enhancement of the Curie constant  $C$ . Simultaneously, the paramagnetic temperature changes sign and  $\Theta_{\text{AFM}} = -(25 \pm 4)$  K [Fig. 5(a)]. However, the antiferromagnetic section of the Curie-Weiss law for  $\text{VO}_x$  NTs is much shorter than for  $\text{VO}_x$  NLS and is limited from below by the power-law onset, similar to that in nanolayers with  $\xi \sim 0.7$  [Fig. 5(b)].

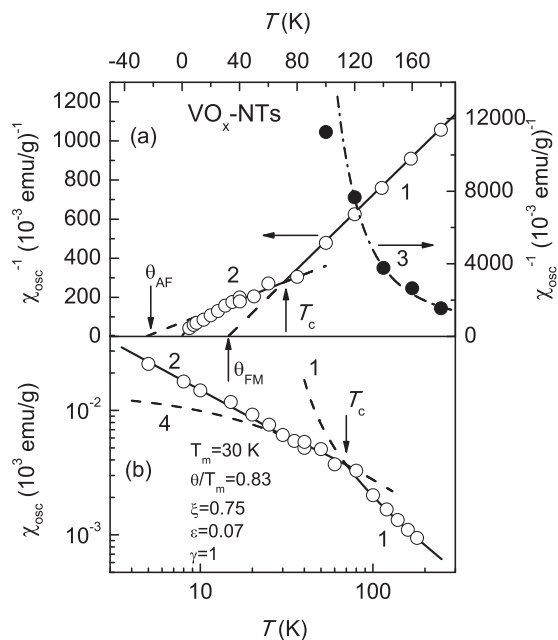


FIG. 5. Temperature dependence of the oscillating part of magnetic susceptibility for the  $\text{VO}_x$  NTs (a) in the Curie-Weiss coordinates and (b) in the logarithmic coordinates. Open circles mark experimental data for line A ( $\text{V}^{4+}$  quasifree spins). Full circles denote experimental data for line B ( $\text{V}^{4+}$ - $\text{V}^{4+}$  antiferromagnetic dimers). Curves 1 are the Curie-Weiss fit in the ferromagnetic region ( $T > T_C$ ); curves 2 are the fit by the quantum critical model for  $T < T_C$ ; curve 3 is the fit by the model of antiferromagnetic dimers (Ref. 7); curve 4 is the Curie-Weiss asymptotic for  $T < T_C$  (see text for details). The paramagnetic temperatures are marked by arrows.

Thus the low-temperature ( $T < T_C$ ) behavior of  $\chi_{\text{osc}}(T)$  for line A is qualitatively the same in  $\text{VO}_x$  NTs and  $\text{VO}_x$  NLS. A characteristic feature of nanotubes consists of a change of both the Curie constants and sign of  $\Theta$  at  $T_C \sim 70$  K. This effect was called FM-AFM crossover in Ref. 7; the possible nature of this phenomenon is discussed in Sec. VI.

#### IV. STATIC AND DYNAMIC MAGNETIC SUSCEPTIBILITIES

In the general case, the total static magnetic susceptibility  $\chi$  and dynamic susceptibility  $\chi_{\text{osc}}$  responsible for the magnetic oscillations are related by the equation

$$\chi(T) = \chi_{\text{osc}}(T) + \chi_b(T), \quad (1)$$

where  $\chi_b$  denotes a part of the total susceptibility, which does not contribute to the observed ESR modes. The physical nature of  $\chi_b(T)$  may be different. For example, this contribution may be caused by the Van Vleck correction either diamagnetic or paramagnetic. In this situation, the sign of  $\chi_b$  could differ and therefore both relations  $\chi_{\text{osc}} < \chi$  and  $\chi_{\text{osc}} > \chi$  are possible. However, there are options when  $\chi_b$  originates from the spin part of the magnetic susceptibility as well as  $\chi_{\text{osc}}$ . In the case of the presence of free electrons in the sample, the Pauli-type susceptibility  $\chi_{\text{Pauli}}$  may contribute to  $\chi_b$  rather than to  $\chi_{\text{osc}}$ . Indeed, assuming that concentrations of the localized magnetic moments (LMMs) and free electrons are the same, the ratio of the corresponding susceptibilities is  $\chi_{\text{Pauli}}/\chi_{\text{LMM}} \sim k_B T/E_F$ ,

i.e., much less than the unity for a degenerate electron gas (here  $E_F$  denotes the Fermi energy). In addition, the possible ESR line, which corresponds to free electrons, would be broader than that for LMMs due to the faster spin diffusion and/or spin fluctuations. As a result, the oscillating part of the magnetic susceptibility, which provides the resonant line in the ESR geometry (the maximal oscillating magnetic field and almost zero electric field), is predominantly controlled by the LMMs,  $\chi_{\text{osc}} \approx \chi_{\text{LMMs}}$ , and the paramagnetic response of free electrons may serve as nonresonant background together with the Landau diamagnetism and the Van Vleck corrections.

When we consider the  $\text{VO}_x$  materials, it is worth noting that there is a trend to treat them as the Mott-Hubbard insulators.<sup>1</sup> In this model, the occupied single electron states in the lower Hubbard band,  $D^1$ , may correspond to  $V^{4+}$  LMMs, whereas the double occupied state in the upper Hubbard band,  $D^2$ , requires opposite spin directions on the V site forming nonmagnetic centers. Therefore the  $D^2$  states likely contribute to the nonoscillating part of susceptibility  $\chi_b$ . If the electron states in the  $D^2$  band are localized, the Van Vleck-type term may be expected for the  $S = 0$  state and, if the upper Hubbard band is delocalized, a Pauli-type contribution occurs.<sup>21</sup>

The examples considered above correspond to the case when the nonresonant part of the susceptibility is formed by some kind of corrections to the main magnetic contribution, which originates from LMMs, and thus a condition  $\chi_{\text{osc}} \approx \chi_{\text{LMM}} > \chi_b$  is valid. This assumption is often made in literature for the description of the susceptibility structure in  $\text{VO}_x$  NTs.<sup>2</sup> However, the above arguments concerning the different linewidths can be applied not only to the case of LMMs and free electrons but also to the situation when the magnetic ions are not equivalent and can be characterized by different spin-fluctuation rates corresponding to both narrow and broad resonant lines. In experimental conditions, the broad line can become undetectable and thus contributes to  $\chi_b$ , whereas the narrow one dominates in the observed ESR spectrum. In the latter case, the susceptibilities  $\chi_{\text{osc}}$  and  $\chi_b$  have either close magnitudes,  $\chi_{\text{osc}} \sim \chi_b$ , or even condition  $\chi_{\text{osc}} \ll \chi_b$  is valid. Thus the procedure of the separation of various contributions to susceptibility becomes ambiguous and both possibilities,  $\chi_{\text{osc}} > \chi_b$  and  $\chi_{\text{osc}} \sim \chi_b$ , must be taken into account.

The comparison of the  $\chi(T)$  data obtained by a SQUID magnetometer with the ESR integrated intensity temperature dependence  $I(T) \propto \chi_{\text{osc}}(T)$  shows that in the case of  $\text{VO}_x$  NLs and  $\text{VO}_x$  NTs, the nonresonant background contribution is not negligible. As long as spin susceptibilities in the studied samples increase as temperature is lowered (Figs. 6 and 7), it is worthwhile to start analysis by normalizing  $I(T)$  on  $\chi(T_{\text{min}})$  values corresponding to the lowest temperature  $T_{\text{min}}$  in the ESR experiment.

It follows from Fig. 6 that for  $\text{VO}_x$  NLs, the aforementioned procedure shows that the normalized  $I(T) = \chi_{\text{osc}}(T)$  curve (open circles 2 in Fig. 6) bends downward with respect to the total susceptibility  $\chi(T)$  (curve 1 in Fig. 6) and hence  $\chi_{\text{osc}}(T) < \chi(T)$  at all temperatures studied. This means that  $\chi_b > 0$  in the studied case. It is interesting that the simplest assumption  $\chi_b = \text{const}$  (curve 3 in Fig. 6) provides a reasonable approximation of the normalized  $I(T)$  data by  $\chi(T) - \chi_b$  (curve 4 in Fig. 6). Thus for  $\text{VO}_x$  NLs, the procedure of separating the oscillating part  $\chi_{\text{osc}}(T)$  from

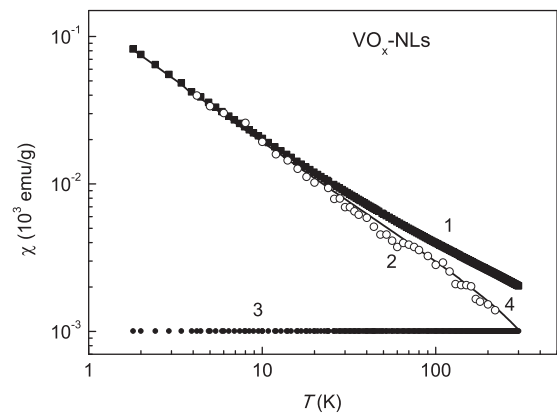


FIG. 6. Static and dynamic magnetic susceptibilities for the  $\text{VO}_x$  NLs. Squares 1 correspond to the total static susceptibility; circles 2 are an absolute calibration of the ESR data; circles 3 are a nonoscillating background. Line 4 is an oscillating part of the magnetic susceptibility calculated from the total static susceptibility for the given background.

the total susceptibility  $\chi(T)$  reduces to the approximation of the  $I(T)$  data obtained in the ESR experiment by the model function  $I_m(T) = A[\chi(T) - \chi_b]$ , which has two fitting parameters,  $A$  (the unknown coefficient of proportionality between  $I$  and  $\chi_{\text{osc}}$ ) and  $\chi_b$ . Figure 6 represents a result of the best fit for the  $\text{VO}_x$ -NLs dynamic susceptibility data together with the total susceptibility  $\chi(T)$  and the background  $\chi_b$ . At all temperatures studied, the condition  $\chi_{\text{osc}} > \chi_b$  is satisfied and these susceptibilities are expected to become comparable at  $T \sim 300$  K (Fig. 6).

The situation with analysis of static and dynamic magnetic susceptibilities for  $\text{VO}_x$  NTs is more complicated. The same procedure suggests that a normalized sum of the integrated intensities for free  $V^{4+}$  ions and AFM dimers,  $I_s(T)$ , exceeds the total static susceptibility in a wide temperature range  $T < T_C$  and becomes less than the  $\chi(T)$  at  $T > T_C$  (Fig. 7), which may correspond to  $\chi_b < 0$  for  $T < T_C$  and  $\chi_b > 0$  for

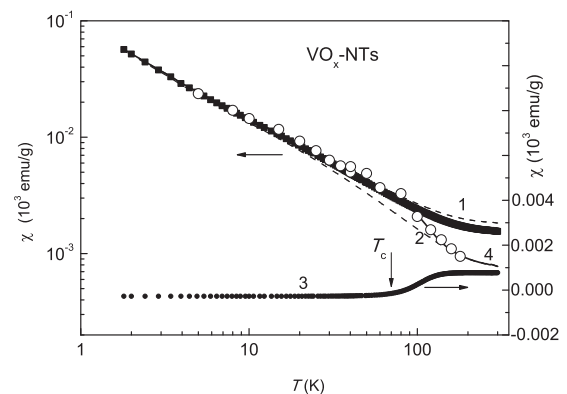


FIG. 7. Static and dynamic magnetic susceptibilities for  $\text{VO}_x$  NTs. Squares 1 correspond to the total static susceptibility; open circles 2 are an absolute calibration of the ESR data; circles 3 are a nonoscillating background. Line 4 is the oscillating part of the magnetic susceptibility calculated from the total static susceptibility for the given background. Dashed lines mark the oscillating part of the magnetic susceptibility in the limits  $T \ll T_C$  and  $T \gg T_C$ .

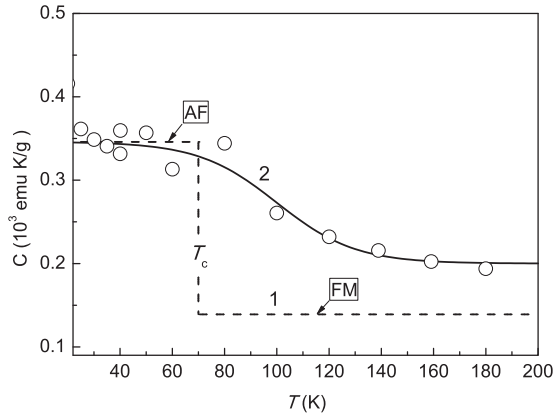


FIG. 8. The Curie constant for  $\text{VO}_x$  NTs. The dashed line 1 corresponds to the FM-AFM crossover scenario; circles and solid line 2 show a scenario of AFM interactions. The solid line corresponds to the background in Fig. 7 (see text).

$T > T_C$ . Following this, we found that a condition  $\chi_b = \text{const}$  is sufficient to describe the  $\chi_{\text{osc}}$  behavior for each temperature interval. Therefore the application of the data analysis schema described above for  $\text{VO}_x$  NLs results in determination of three parameters:  $A$  (which is the same in both temperature intervals),  $\chi_b(T < T_C) < 0$ , and  $\chi_b(T > T_C) > 0$ . The total curve  $\chi_{\text{osc}}(T)$  can be simulated assuming a transition from a high-temperature to a low-temperature asymptotic in the vicinity of  $T_C$ :

$$\chi_{\text{osc}} = [\chi(T) - \chi_b(T > T_C)]\varphi(T) + [\chi(T) - \chi_b(T < T_C)][1 - \varphi(T)], \quad (2)$$

where the function  $\varphi(T)$  satisfies the conditions  $\varphi(T \gg T_C) = 1$  and  $\varphi(T \ll T_C) = 0$ . The final result of the analysis is presented in Fig. 7. The model form  $\varphi(T) = \tanh[(T - T^*)/\delta]$  with  $T^* = 100$  K and  $\delta = 30$  K has been used for calculation. The suggested procedure allows obtaining approximation of  $I_s(T)$  by the  $\chi_{\text{osc}}(T)$  curve for  $\text{VO}_x$  NTs with a reasonable accuracy.

The obtained coefficients  $A$  for  $\text{VO}_x$  NLs and  $\text{VO}_x$  NTs give an absolute calibration of the integrated intensity in the units of magnetic susceptibility and thus gives  $\chi_{\text{osc}}$  in absolute units used in Figs. 4 and 5. The use of the absolute calibration and quantum critical model described in the next section allows finding values of the Curie constants. For the quasifree spins in  $\text{VO}_x$  NLs this parameter equals  $C = (3.34 \pm 0.04) \times 10^{-4}$  emu K/g. In the case of  $\text{VO}_x$  NTs data analysis gives  $C_d = (6.21 \pm 0.08) \times 10^{-3}$  emu K/g for AFM dimers, whereas for quasifree spins the Curie constants are  $C = (1.39 \pm 0.03) \times 10^{-4}$  emu K/g and  $C = (3.46 \pm 0.07) \times 10^{-4}$  emu K/g for the intervals  $T > T_C$  and  $T < T_C$ , respectively.

We see that the antiferromagnetic Curie-Weiss law for both  $\text{VO}_x$  NTs and  $\text{VO}_x$  NLs is not only characterized by close paramagnetic temperatures but also possesses almost coinciding Curie constants. It is also worth noting that both  $\text{VO}_x$  NTs and  $\text{VO}_x$  NLs demonstrate the same low-temperature anomaly (Figs. 4 and 5). In addition, in  $\text{VO}_x$  NTs and  $\text{VO}_x$  NLs, the absolute values of the nonoscillating contribution  $\chi_b$  are of the same order (Figs. 6 and 7).

The considered procedure of separating of the magnetic contributions in  $\text{VO}_x$  NTs corresponds to the case  $\chi \sim \chi_{\text{osc}} > \chi_b$ , when  $\chi_b$  can be considered as some kind of correction to the main LMM contribution. Formally, it is possible to obtain an approximation for  $\chi_{\text{osc}}$  under the opposite assumption  $\chi \sim \chi_b \gg \chi_{\text{osc}}$ . This route was chosen in Ref. 14 and brought a result that the oscillating part of the magnetic susceptibility does not exceed 2–20% of  $\chi(T)$  for  $\text{VO}_x$  NTs. However, in our opinion, the assumption used in Ref. 14 contradicts experimental data for  $\text{VO}_x$  NTs and  $\text{VO}_x$  NLs. Indeed, if the separation of magnetic contributions suggested in Ref. 14 is correct, the  $\chi_{\text{osc}}$  is noticeably reduced in  $\text{VO}_x$  NTs by a factor of 5–50 with respect to  $\chi_{\text{osc}}$  in  $\text{VO}_x$  NLs. Thus as long as the average charge of vanadium is almost the same,  $\zeta = +(4.2 \dots 4.3)$  in  $\text{VO}_x$  NTs and  $\text{VO}_x$  NLs and the chemical composition of these materials is very close (see Sec. II), the integrated intensity of the ESR signal must be considerably less in the  $\text{VO}_x$  NT sample, which has the same mass as the  $\text{VO}_x$ -NL sample. This behavior does not meet the experimental situation where the ESR signals for the similar samples of  $\text{VO}_x$  NLs and  $\text{VO}_x$  NTs are comparable. Therefore we believe that the procedure of separating the magnetic contributions proposed in the present work and shown in Fig. 7 is more correct than that implied in Ref. 14. Moreover, the close  $\zeta$  values and close chemical composition strongly support an idea of the presence of the certain similarity of magnetic subsystems of  $\text{VO}_x$  NTs and  $\text{VO}_x$  NLs. As we can see from the estimates of the Curie constants, this similarity indeed takes place in the low-temperature region but only in the case when the relation  $\chi \sim \chi_{\text{osc}} >$  holds for both nanomaterials studied and results in the behavior of the magnetic susceptibility shown in Figs. 6 and 7.

## V. LOW-TEMPERATURE ANOMALY

The observation of the magnetic susceptibility power law in  $\text{VO}_x$  NLs and  $\text{VO}_x$  NTs at low temperatures may indicate an onset of a disordered-driven quantum critical (QC) regime.<sup>9–13</sup> This hypothesis was first formulated in Ref. 6 for  $\text{VO}_x$  NTs. Theoretically, in the case of the QC regime induced by disorder, the ground state is represented by the Griffiths phase consisting of spin clusters characterized by different values of the exchange integral  $J$ .<sup>9–11</sup> The magnetic susceptibility in the Griffiths phase at low temperatures obeys the power law  $\chi \propto 1/T^\xi$  ( $\xi < 1$ ), which is different from the Curie-Weiss dependence. This law is a consequence of the power distribution function of exchange energies and reflects low-temperature correlations in a spin system.

As is often observed in experiments on disorder-driven QC systems, the high-temperature Curie-Weiss law somehow transforms at  $T \sim T_G$  to a power law as temperature is lowered. The  $\chi(T)$  sections for  $T < T_G$  and  $T > T_G$  tend to be treated separately and only the region  $T < T_G$  is considered as relevant to the QC phenomena. However, as long as distribution function of  $J$  exists at all temperatures, it can affect both low-temperature (correlated QC spin clusters) and high-temperature (quasifree spins) magnetic properties. In this sense, the high-temperature region also contains information on the QC regime.

Unfortunately, the explicit evaluation of the  $\chi(T)$  for the QC system is hardly possible at an arbitrary temperature

and thus only the low-temperature ( $T \rightarrow 0$ ) asymptotics are obtained in most of the works.<sup>9–11</sup> An approach, which allows describing the magnetic susceptibility of a disorder-driven QC system with AFM interactions at an arbitrary temperature, has been recently suggested in Refs. 12 and 13. In this model, a disordered magnetic system is considered as a set of identical volume elements, each characterized by the Néel temperature  $T_N \sim J$  and the paramagnetic temperature  $\Theta = -T_N/\varepsilon$ . For the three-dimensional antiferromagnet, the parameter  $\varepsilon$  can be expressed through the molecular-field constants,<sup>22</sup> but in the model<sup>14,20</sup> it has a more general sense being a degree of suppression of an ordering temperature.

The magnetic susceptibility of each volume element at  $T > T_N$  is described by the Curie-Weiss dependence<sup>13</sup>

$$\chi = C/(T + T_N/\varepsilon), \quad (3)$$

and decreases at  $T < T_N$  according to the law

$$\chi = \frac{C(T/T_N)^\gamma}{T_N(1 + 1/\varepsilon)}. \quad (4)$$

Apart from the standard values  $\gamma = 0$  and  $\gamma = 1$ ,<sup>22</sup> the case  $\gamma \gg 1$ , which simulates the opening of the spin gap, can be considered.<sup>12,13</sup> In the described model, the Curie constant  $C$  and parameter  $\varepsilon$  are taken identical for all volume elements, and the Néel temperature  $T_N$  for a volume element is a random quantity limited from above,  $T_N < T_m$ , with the distribution function<sup>13</sup>

$$w(T_N) = (1 - \xi)(T_m/T_N)^\xi/T_m. \quad (5)$$

Then, the magnetic susceptibility of the system is given by<sup>13</sup>

$$\chi = \begin{cases} C/(T - \Theta), & T > T_m, \\ \frac{C}{T_m - \Theta} \left(\frac{T_m}{T}\right)^\xi F(\varepsilon, \xi, \gamma, T_m, T), & T < T_m, \end{cases} \quad (6)$$

$$F = 1 + \frac{(1 - \xi)(1 - \Theta/T_m)}{(1 + 1/\varepsilon)(\gamma + \xi)} \left[ 1 - \left(\frac{T}{T_m}\right)^{\gamma + \xi} \right]. \quad (7)$$

The effective paramagnetic temperature  $\Theta$  in Eqs. (6) and (7) can be found analytically,

$$\Theta/T_m = [\varepsilon(\xi - 1)f(\varepsilon, \xi)]^{-1} \quad (8)$$

where

$$f(\varepsilon, \xi) = -\frac{1}{\xi} - \sum_{r=1}^{\infty} (-1)^r \frac{\varepsilon^r}{r + \xi} + \frac{\pi}{\varepsilon^\xi \sin[\pi(1 - \xi)]}. \quad (9)$$

For  $T > T_m$ , the Curie-Weiss law with the effective AFM temperature is exact and a decrease in temperature in the range  $T < T_m$  results in “scanning” over the random  $T_N$  of volume elements. If  $T < T_N$ , the magnetic contribution of the corresponding volume elements freezes out due to the transition to the magnetically ordered state and the Curie-Weiss behavior gives way to the power dependence of the magnetic susceptibility for the whole sample. Therefore the spin clusters with higher degree of correlation (in comparison with the average value), which determine the Griffiths phase magnetic properties according to Refs. 9–11, should be considered as sets of volume elements for which  $T_N > T$ . Apparently, a local magnetic ordering in the elementary volumes in the considered

model does not suggest an onset of any long-range magnetic order in the real experimental system.<sup>12,13</sup>

For the approximation of  $\chi(T)$  experimental data for  $\text{VO}_x$  NLs and  $\text{VO}_x$  NTs with Eqs. (6)–(9), the following method was used. In a temperature region where the Curie-Weiss law is valid, the two-parameter fits allow finding  $C$  and  $\Theta = \Theta_{\text{AFM}}$ . The low-temperature part of  $\chi(T)$  depends on four parameters, namely,  $\xi$ ,  $\varepsilon$ ,  $\gamma$ , and  $T_m$  [Eqs. (6b) and (7)]. However, as long as  $\Theta$  is fixed, the variables  $\xi$ ,  $\varepsilon$ , and  $T_m$  are determined by Eqs. (8) and (9), and hence there are only three independent parameters left for fitting the  $\chi(T)$  section with the power law. For example, excluding  $T_m$  using Eq. (8), we can reduce Eqs. (6b) and (7) to the form  $\chi(\varepsilon, \xi, \gamma, T)$ , which can be applied for fitting the experimental data. Further simplification is coming from the fact that within accuracy better than 1% in the range  $\varepsilon < 0.5$  it is sufficient to take the first three terms of the infinite sum in Eq. (9). Additionally, the parameter  $\gamma$  defines the transition region from the Curie-Weiss law to the power law and thus weakly affects the  $\chi(T)$  behavior at low temperatures. Therefore it is reasonable to restrict  $\gamma$  to a fixed value chosen from “physical model” arguments, i.e.,  $\gamma = 0$  and  $\gamma = 1$  (the antiferromagnetic cluster model<sup>22</sup>) and  $\gamma \sim 10$  (the spin gap model<sup>12,13</sup>). The choice of a particular value of  $\gamma$  can be made from a criterion of the best reproduction of the transition area of the  $\chi(T)$  curve. Thus the fitting of the low-temperature part of  $\chi(T)$  in practice reduces to a problem of the two-parameter fit. The procedure considered above may be used for obtaining of the reasonable values of the first approximation for the parameters appearing in the model. The values obtained may be improved further by application of an iteration method. It is worth noting that as long as expression (6) is applied to the whole temperature range the reliability of determination of Curie constant in the suggested ansatz is higher than in the case of the standard fitting of linear section of the  $\chi^{-1} = f(T)$  curve.

The results of fitting the magnetic susceptibility of the  $\text{V}^{4+}$  quasifree spins are presented by solid lines in Fig. 4 for  $\text{VO}_x$  NLs and in Fig. 5 for  $\text{VO}_x$  NTs. The procedure considered above provides a reasonable description of the experimental data within the QC model, which assumes disorder-driven decomposition of the  $\text{V}^{4+}$  magnetic subsystem into spin clusters. From the best fit, the following parameter sets were obtained:  $T_m = 51.6 \pm 2.5$  K,  $\xi = 0.85 \pm 0.015$ ,  $\varepsilon = 0.11 \pm 0.01$  for  $\text{VO}_x$  NLs and  $T_m = 30.0 \pm 3$  K,  $\xi = 0.75 \pm 0.03$ ,  $\varepsilon = 0.075 \pm 0.006$  for  $\text{VO}_x$  NTs. For both nanomaterials, the best approximation was achieved for  $\gamma = 1$  (the case of the AFM cluster model). The values of corresponding Curie constants were given in the previous section.

The carried out analysis of the magnetic susceptibility data supports the interpretation of an anomalous power law  $\chi(T) \propto 1/T^\xi$  by a disorder-driven quantum criticality. The appearance of the disorder-driven QC phenomena in the samples studied is related to a certain amount of a structural disorder (see Sec. II and Fig. 1), which may induce a disorder in magnetic interactions in the  $\text{VO}_x$  plane. In the considered model, the disorder rate can be associated either with the distribution function exponent  $\xi$  or with the suppression parameter  $\varepsilon$ : the less are  $\xi$  and  $\varepsilon$ , the higher is disorder in the magnetic subsystem. From this point of view,  $\text{VO}_x$  NTs are more disordered than  $\text{VO}_x$  NLs, probably because of imperfect

scrolling and scrolling-induced stresses in the  $\text{VO}_x$  plane. The presence of AFM dimers may be considered as an extra disorder source in  $\text{VO}_x$  NTs, as long as dimers may affect spatial distribution and magnetic interactions of the quasifree spins. According to Refs. 12 and 13, the parameter  $T_m$  may serve as an estimate of the maximal exchange constant  $J_m \sim T_m$  corresponding to the magnetic system without disorder. It is supposed that in a QC disorder-driven system, the disorder likely tends to decrease the exchange constants in the sample volume ( $J < J_m$ ) resulting in the system decomposition into spin clusters. Consequently, the exchange constant is expected to be higher in  $\text{VO}_x$  NLs than that in  $\text{VO}_x$  NTs. This prediction can be verified by neutron-scattering experiments interesting for future investigations.

## VI. CURIE CONSTANTS, FM-AFM CROSSOVER, AND CONCENTRATION ESTIMATES

The effect of the FM-AFM crossover is characteristic to  $\text{VO}_x$  NTs and consists of a change of the sign of the paramagnetic temperature accompanied by variation of the Curie constant describing a temperature dependence of  $\chi_{\text{osc}}$  for  $T < T_C$  and  $T > T_C$  (Fig. 5). Taking into account the fact that the amplitude of the elementary oscillating magnetic moment does not depend on temperature, this effect was explained in Ref. 7 by an abrupt increase in the concentration of  $\text{V}^{4+}$  localized magnetic moments at  $T_C$  resulting in a stepwise enhancement of the Curie constant (curve 1 in Fig. 8). According to Ref. 7, the increase in the number of LMMs, in turn, is due to capturing the quasifree electrons and their localization at  $\text{V}^{5+}$  nonmagnetic ions, i.e., is caused by the process  $\text{V}^{5+} + e \rightarrow \text{V}^{4+}$ . Consequently, a presence of these electrons in the  $\text{VO}_x$  nanomaterial is to be postulated.<sup>7</sup>

Let us consider a possible Pauli-type contribution to the background  $\chi_b$ . As long as the Pauli susceptibility is proportional either to the concentration of free-band electrons or to the concentration of the delocalized electrons in the upper Hubbard band, the variation of this parameter induces a change in  $\chi_b$ . Moreover,  $\chi_b$  decreases with lowering temperature (Fig. 7), which corresponds to decreasing the free-electron concentration  $n_e$  and freezing out the Pauli term (Fig. 7). Consequently, the change in the  $\chi_b$  sign in the considered model may be explained by an interplay between the Van Vleck diamagnetism  $\chi_0$  and the Pauli term  $\chi_{\text{Pauli}}$  of comparable amplitude. For example, assuming a complete localization of free electrons below  $T_C$ , we can expect  $\chi_b(T < T_C) \approx \chi_0 < 0$  and  $\chi_b(T > T_C) \approx \chi_0 + \chi_{\text{Pauli}} > 0$ .

However, the obtained temperature dependence of  $\chi_b$  is not abrupt and the nonoscillating part of the susceptibility varies at  $T > T_C$  (Fig. 7). Thus the correlated change in LMMs and free-electron concentration should occur in the FM region of the  $\chi(T)$  curve. In order to keep the linear temperature dependence of  $\chi^{-1}(T)$  with the observed parameters  $C$  and  $\Theta_{\text{FM}}$  [Fig. 5(a)], it is essential to believe that there is a temperature dependence of the paramagnetic temperature, which exactly compensates the change in  $C(T)$ . Such supposition appears as an *ad hoc* assumption and looks unlikely. Another difficulty in treatment of the FM-AFM crossover suggested in Ref. 7 is the absence of a microscopic mechanism responsible for the change in magnetic interaction type at  $T_C$ .

The data on the structure of magnetic susceptibility (Fig. 7), obtained in the present work, allows suggesting a different interpretation of the crossover effect. Let us suppose magnetic interaction between quasifree spins in  $\text{VO}_x$  NTs remaining antiferromagnetic in the whole temperature range and being characterized by the same paramagnetic temperature  $\Theta_{\text{AFM}} = -25$  K as below  $T_C$ . Therefore the dynamic susceptibility acquires the form  $\chi_{\text{osc}} = C(T)/(T - \Theta_{\text{AFM}})$  with the temperature-dependent Curie constant. When temperature is lowered, the Curie constant  $C(T)$  increases  $C(T) \propto N_{\text{V}^{4+}}(T) = N_0 - \Delta n_e(T)$  due to the process of electron localization  $\text{V}^{5+} + e \rightarrow \text{V}^{4+}$ . Here  $N_{\text{V}^{4+}}$  is the concentration of the  $\text{V}^{4+}$  LMMs at arbitrary temperature,  $N_0$  stands for the concentration of LMMs at low temperatures  $T \ll T_C$  and  $\Delta n_e(T)$  denotes a part of the free-electrons concentration, which undergo localization process. Assuming that  $\chi_b = \chi_0 + \chi_{\text{Pauli}}$  and taking the Pauli term variation  $\Delta \chi_{\text{Pauli}}(T)$  being proportional to  $\Delta n_e(T)$  into account, we see that  $C(T)$  follows the same functional dependence as  $\chi_b(T)$  [see Eq. (2)] but of opposite sign.

The  $C(T)$  values obtained from  $\chi_{\text{osc}}(T)$  together with the model temperature dependence subtracted from  $\chi_b$  as described above are presented in Fig. 8 (circles and curve 2, respectively). As can be seen, the temperature-dependent part of  $\chi_b$  reasonably describes the shape of the  $C(T)$  curve. The fitting of  $C(T)$  data with an analog of Eq. (2), with the same model choice for  $\varphi(T)$ , and with the same values of  $T^*$  and  $\delta$  as for  $\chi_b$  allows estimating  $C(T \gg T_C) = 2 \times 10^{-4}$  emu K/g in the model of the AFM interacting LMMs (Fig. 8).

The suggested approach allows describing both  $\chi_b(T)$  and  $\chi_{\text{osc}}(T)$  in a reliable way without changing the magnetic interaction type at  $T_C$ . Thus  $\text{VO}_x$  NTs, as well as the  $\text{VO}_x$  NLs, can be treated as antiferromagnets in the whole temperature range studied. From this point of view, an essential difference between  $\text{VO}_x$  NTs and  $\text{VO}_x$  NLs consists of the process of electron localization (capturing of quasifree electrons by nonmagnetic  $\text{V}^{5+}$  sites) with decreasing temperature, that is specific to  $\text{VO}_x$  NTs and is missing in  $\text{VO}_x$  NLs. In  $\text{VO}_x$  NTs, this process likely emulates the FM-type Curie-Weiss dependence for  $\chi_{\text{osc}}$  in a transition temperature region. It is worth noting that the existence of a similar “quasiferromagnetic” transition region has been recently reported for the  $\text{VO}_x$  nanorods,<sup>5</sup> which may indicate that possible effects of electron localization may be relevant for various vanadium oxide nanomaterials.

The above consideration shows essential difficulties in correct determination of the concentrations for various spin species in  $\text{VO}_x$  nanomaterials, when straightforward use of the Curie constants leads to controversial estimates. For example, for  $\text{VO}_x$  NTs the magnetic susceptibility  $\chi(T)$  data fitting in Ref. 2, performed by the superposition of the Curie-Weiss law and the model of noninteracting AFM dimers in the range  $T > 15$  K gives about 17% and 28% of the total V sites corresponding to the quasifree spins and AFM dimers. The rest of the V sites is supposed to correspond to nonmagnetic  $\text{V}^{5+}$  ions with spin  $S = 0$ . From the other hand, the analysis of the field dependence of magnetization at  $T = 4.2$  K implies the concentration of the quasifree spins being only about 3%.<sup>2</sup>

All concentration estimates, reported in literature, were carried out in the assumption that the magnetic subsystem only

consists of  $V^{4+}$  states (one electron localized at the  $V^{5+}$  site) and empty  $V^{5+}$  sites. In these calculations, the complicated magnetic susceptibility structure and a possible contribution of free electrons were not taken into account as well as the experimental difference in the  $g$  factors for the quasifree spins and AFM dimers. Additionally, the magnetic properties analysis must be consistent with the results of the chemical analysis including the average charge of the vanadium ion.

We start our analysis from the obvious equation for the average vanadium charge,

$$\zeta = 5 - x = 5 - (x_l + x_e) = 5 - (x_f + x_d + x_e), \quad (10)$$

which assumes that there are  $x$  electrons per bare vanadium site with  $\zeta_0 = +5$  making the observed value of  $\zeta$ . In turn, the reduced concentration  $x$  may be subdivided into the contribution  $x_l$  of the electrons localized at  $V^{5+}$  sites forming magnetic  $V^{4+}$  states (these electron states are observed in ESR) and contribution  $x_e$ , which corresponds to either free-band electrons or to the electrons in the upper Hubbard band. According to the results of the present work and literature data,<sup>1,2,6,7</sup> the localized electrons consist of quasifree spins with the reduced concentration  $x_f$  and dimers with the reduced concentration  $x_d$ .

The concentrations  $x_f$  and  $x_d$  can be found from the corresponding Curie constants for the quasifree spins and dimers:

$$C = \frac{N_A \mu_B^2}{k_B m} g_f^2 \frac{S(S+1)}{3} x_f = \frac{N_A \mu_B^2}{4k_B m} g_f^2 x_f, \quad (11)$$

$$C_d = \frac{N_A \mu_B^2}{k_B m} g_d^2 x_d, \quad (12)$$

where  $m$  denotes the molecular mass of the  $VO_x$  nanomaterial,  $g_f = 1.96$  and  $g_d \approx 2.5$  are related  $g$  factors,  $N_A$  is the Avogadro number,  $\mu_B$  is the Bohr magneton, and  $k_B$  is the Boltzmann constant. Therefore Eqs. (10)–(12) allow calculating all three parameters for the experimental values  $C$  and  $C_d$  obtained in the various models (see Sec. VI). The results are presented in Table I. Together with the  $x_f$ ,  $x_d$ , and  $x_e$ , the reduced number of empty  $V^{5+}$  sites,  $x_{\text{empty}} = 1 - (x_f + x_d + x_e)$ , is shown.

In  $VO_x$  NTs, the concentration of the AFM dimers is high and almost half of the vanadium sites are dimerized. The concentration of the quasifree spins is noticeably lower than that of dimers in both temperature intervals,  $T < T_C$  and  $T > T_C$ . The ratio  $x_d/x_f$  reaches 2.7 at low temperatures ( $T < T_C$ ) and is about 4.9–7.0 at high temperatures ( $T > T_C$ )

depending on the model used. It is worth noting that at  $T > T_C$ , the absolute values of  $x_f$  and  $x_e$  in the FM-AFM crossover model and in the model of AFM interactions differ by 3% only. At the same time, the ratio  $x_e/x_f$  at  $T > T_C$  is more sensitive to the model used and equals 1.9–3.1.

The characteristic feature of  $VO_x$  NTs consists of the validity of the inequality  $x_l = x_f + x_d > x_e$  at all temperatures. The number of electrons forming the  $V^{4+}$  LMMs is 2.5–6.0-fold higher than the number of electrons contributing to the nonresonant background. It follows from Table I that the situation is just opposite in  $VO_x$  NLs:  $x_l = x_f + x_d < x_e$ , and the ratio  $x_l/x_e$  is about 0.4 in this nanomaterial. Thus  $VO_x$  NLs differ from  $VO_x$  NTs not only by the absence of AFM dimers, but also by 2–4-fold higher concentration  $x_e$ .

Let us consider the obtained concentration estimates in the framework of the Mott-Hubbard concept.<sup>1</sup> According to the structural studies,<sup>1,2,18</sup> the  $VO_x$  plane is close to that in  $BaV_2O_{16} \cdot nH_2O$  and thus there are seven vanadium sites of three types, V(1), V(2), and V(3) in the unit cell. Three V(1) sites and three V(2) sites correspond to the octahedral coordination and form zigzag chains in double  $VO_x$  layers,<sup>1,2,18</sup> whereas the remaining V(3) site corresponds to the tetrahedral coordination and is located between the layers formed by V(1) and V(2) sites. The treatment of  $VO_x$  NTs as the Mott-Hubbard material was carried out in Ref. 1 assuming (i) the energy scale hierarchy  $E_{V(1)} > E_{V(2)} > E_{V(3)}$  and (ii) the only presence of  $D^1$  and  $D^2$  states of the V(1) sites separated by an energy gap in the vicinity of the Fermi level. As long as there are 43% of V(1), 43% of V(2), and 14% of V(3) sites in the sample, this spectrum suggests the number of the observed LMMs being not less than 57%. This makes it difficult to explain the LMM concentration in  $VO_x$  NLs, where the  $VO_x$  plane is essentially the same as in  $VO_x$  NTs. Moreover, the presence of two substantially different types of LMMs, which correspond to V(1,2) and V(3) sites, leads to different ESR characteristics like the  $g$  factor and linewidth, which does not meet the experimental situation where a single nearly Lorentzian line is observed (Figs. 2 and 3). In addition, it is not clear why V(1) and V(2) sites in a close structural surrounding have so different energies as supposed in Ref. 1.

The data in Table I show that the experimental concentration of the LMMs is always less than the maximal possible number of  $V^{4+}$  sites given by an average charge  $\zeta$ . In the Mott-Hubbard model this discrepancy should be attributed to the presence of the  $D^2$  nonmagnetic states at the Fermi level, i.e., the  $D^1$  and  $D^2$  states overlap. This situation looks very unusual even if the lower and upper Hubbard bands are formed by V(1,2) sites

TABLE I. Concentration estimates.

Concentration		Sample			
		$VO_x$ NLs	$VO_x$ NTs ( $T < T_C$ )	$VO_x$ NTs ( $T > T_C$ ) <sup>a</sup>	$VO_x$ NTs ( $T > T_C$ ) <sup>b</sup>
LMMs {	$x_f$	0.2	0.18	0.07	0.10
	$x_d$	0	0.49	0.49	0.49
	$x_e$	0.46	0.11	0.22	0.19
	$x_{\text{empty}}$	0.34	0.22	0.22	0.22

<sup>a</sup>FM-AFM crossover.

<sup>b</sup>AFM interactions.

and  $V(3)$  states lies higher in energy and are empty. Thus a theoretical justification of the Mott-Hubbard model applicability to describe the magnetic properties of the  $VO_x$  nanomaterials is required. This task is beyond the scope of the present paper. However, when assuming that the Mott-Hubbard approach works, it is possible to make the following remarks.

If the Hubbard bands originate from the  $V(1,2)$  sites, it is reasonable to expect that the number of electrons and the number of sites in the  $VO_x$  plane do not coincide in the  $D^2$  band (see Table I). Therefore, following Nagaoka's arguments,<sup>21,23</sup> the conductivity of electrons, which does not contribute to the  $V^{4+}$  LMMs, acquires a metallic character as expected from the experimental data analysis.

It is possible to conclude from the above consideration that the filling of the upper Hubbard band  $D^2$  is higher in  $VO_x$  NLs than in  $VO_x$  NTs, which results in increasing  $x_e$ . Consequently, an increase in the conductivity of  $VO_x$  NLs compared to that of  $VO_x$  NTs is expected due to a higher value of  $x_e$  and a metallic character of the  $D^2$  state. Our study of the THz conductivity of these nanomaterials has confirmed this conclusion. The full details of conductivity measurements in  $VO_x$  NTs and  $VO_x$  NLs will be published later.

In the Mott-Hubbard model, the process of an electron capturing by the  $V^{5+}$  site,  $V^{5+} + e \rightarrow V^{4+}$ , corresponds to the decay of the  $D^2$  state into two  $D^1$  states. Therefore the observation of the FM-AFM crossover effect indicates a possible temperature-dependent shift of equilibrium between  $D^1$  and  $D^2$  states. As a likely reason of this behavior, a broad structural transition around  $T_C$  may be considered and hence structural studies of these nanomaterials at low temperatures may be rewarding.

The expected overlap of the Hubbard bands requires a strong reduction of the Coulomb repulsion energy, possibly accompanied by  $D^1$  and  $D^2$  state broadening due to disorder effects. The low repulsion energy is known to favor AFM ordering rather than FM ground state.<sup>21,23</sup> In the samples studied, the long-range magnetic order is suppressed by disorder effects (Sec. V) but the same arguments as in Refs. 21 and 23 suggest the AFM interaction being dominant. Therefore the interpretation of the  $\chi_{osc}$  temperature dependence based on the change of the magnetic interaction type<sup>7</sup> in the Mott-Hubbard-type model appears to be unlikely, and the scenario based on AFM interactions holding in the whole temperature range looks more realistic.

## VII. CONCLUSIONS

We have shown that the magnetic susceptibility in the  $VO_x$  nanolayers and  $VO_x$  nanotubes contains several contributions. Apart from the oscillating susceptibility, which is responsible for the observed ESR modes and corresponds to the localized magnetic moments of the  $V^{4+}$  ( $S = 1/2$ ) ions, there is a nonoscillating background likely formed by the Van Vleck-type and Pauli-type terms. The comparative analysis of the ESR data together with various contributions to the magnetic susceptibility has allowed elucidating effects of scrolling the nanolayers into nanotubes. First, scrolling leads to formation of the antiferromagnetic dimers consisting of almost half of the vanadium ions with a spin gap near 720 K, which are

present in  $VO_x$  nanotubes and are missing in  $VO_x$  nanolayers. The assumption that dimers in nanotubes appear as a result of scrolling of the  $VO_x$  plane provides a hint for the reason of the renormalization of the  $g$ -factor value for these spin species. The scrolled plane should be stressed and formation of the dimers in  $VO_x$  NTs may be considered as a reaction on the stresses. Redistribution of the stresses field in the sample volume may lead to the situation when the stresses and (or) crystalline surrounding around the dimers should be different from the rest of the plane. As long as the splitting of the levels of a spin cluster in magnetic field depends on the local stresses and crystal field, the  $g$ -factor change may occur in agreement with experimental observation.

The second effect, specific to the  $VO_x$  nanotubes, consists of the correlated change in the Curie constant for the nondimerized  $V^{4+}$  quasifree spins and in variations of the background: the decreasing temperature in the interval  $70 \text{ K} < T < 120 \text{ K}$  induces an initial 1.8-fold growth of the Curie constant followed by a decrease, along with a change of the sign of the nonoscillating background. Third, it is found that scrolling results in reduction of the quasifree electron concentration in the  $VO_x$  plane by a factor of 2–4.

A characteristic feature of  $VO_x$  nanolayers and nanotubes is a discrepancy between the maximal possible concentration of the  $V^{4+}$  magnetic ions, which is allowed by chemical composition, and the concentration of the localized magnetic moments. The number of electrons in the  $V^{4+}$  state is always less than the total electron concentration, and the concentration of the “excessive” electrons may vary in the range 0.11–0.46 per vanadium site. This situation may be explained by the unusual overlap of the upper metallic Hubbard band and the lower Hubbard band due to disorder effects and reduction of the on-site Coulomb repulsion energy. The considered case corresponds to the AFM interactions; however, instead of establishing the long-range magnetic order, the possible disorder driven quantum critical phenomena and a transition to the Griffiths phase take place. An experimental consequence of this scenario is the observation of the low-temperature power law of magnetic susceptibility in the  $VO_x$  nanolayers and nanotubes,  $\chi \propto 1/T^\xi$ , with the exponent  $\xi \sim 0.7$ –0.8.

The specific combination of the possible Mott-Hubbard effects, quantum critical phenomena, and influence of disorder show that a development of the adequate theory of magnetism for the nanomaterials studied here is required for the explanation of their unusual magnetic properties.

## ACKNOWLEDGMENTS

Support from the Federal Program “Scientific and Educational Human Resources of Innovative Russia,” from RAS Programs “Strongly Correlated Electrons,” “Quantum Physics of Condensed Matter,” and from the RFBR (Grant No. 09-03-00602-a) is acknowledged. This work was partly supported by a Grant-in-Aid for Creative Scientific Research (Grant No. 19GS1209) from the Japan Society for the Promotion of Science. One of the authors (S.V.D.) would like to thank the Molecular Photoscience Research Center, Kobe University, for financial support.

\*demis@lt.gpi.ru

- <sup>1</sup>L. Krusin-Elbaum, D. M. Newns, H. Zeng, V. Derycke, J. Z. Sun, and R. Sandstrom, *Nature (London)* **431**, 672 (2004).
- <sup>2</sup>E. Vavilova, I. Hellmann, V. Kataev, C. Täschner, B. Büchner, and R. Klingeler, *Phys. Rev. B* **73**, 144417 (2006).
- <sup>3</sup>K. W. Lee, E. M. Lee, H. Kweon, J. Park, and C. E. Lee, *J. Korean Phys. Soc.* **49**, 1625 (2006).
- <sup>4</sup>H. Kweon, K. W. Lee, E. M. Lee, J. Park, I.-M. Kim, C. E. Lee, G. Jung, A. Gedanken, and Y. Koltypin, *Phys. Rev. B* **76**, 045434 (2007).
- <sup>5</sup>J. Park, I. H. Oh, E. Lee, K. W. Lee, C. E. Lee, K. Song, and Y.-J. Kim, *Appl. Phys. Lett.* **91**, 153112 (2007).
- <sup>6</sup>S. V. Demishev, A. L. Chernobrovkin, E. A. Goodilin, V. V. Glushkov, A. V. Grigorieva, N. A. Samarin, N. E. Sluchanko, A. V. Semeno, and Y. D. Tretyakov, *Phys. Status Solidi* **2**, 221 (2008).
- <sup>7</sup>S. V. Demishev, A. L. Chernobrovkin, V. V. Glushkov, A. V. Grigorieva, E. A. Goodilin, N. E. Sluchanko, N. A. Samarin, and A. V. Semeno, *JETP Lett.* **91**, 11 (2010).
- <sup>8</sup>K. W. Lee, H. Kweon, and C. E. Lee, *J. Korean Phys. Soc.* **53**, 3493 (2008).
- <sup>9</sup>R. B. Griffiths, *Phys. Rev. Lett.* **23**, 17 (1969).
- <sup>10</sup>A. J. Bray, *Phys. Rev. Lett.* **59**, 586 (1987).
- <sup>11</sup>D. S. Fisher, *Phys. Rev. Lett.* **69**, 534 (1992).
- <sup>12</sup>S. V. Demishev, *Phys. Solid State* **51**, 547 (2009).
- <sup>13</sup>S. Demishev, *Phys. Status Solidi B* **247**, 676 (2010).
- <sup>14</sup>S. V. Demishev, A. L. Chernobrovkin, V. V. Glushkov, E. A. Goodilin, A. V. Grigorieva, T. V. Ishchenko, A. V. Kuznetsov, N. E. Sluchanko, Y. Tretyakov, and A. V. Semeno, *Fullerenes, Nanotubes, Carbon Nanostruct.* **19**, 27 (2011).
- <sup>15</sup>M. Roppolo, C. B. Jacobs, S. Upreti, N. A. Chernova, and M. S. Whittingham, *J. Mater. Sci.* **43**, 4742 (2008).
- <sup>16</sup>A. V. Grigoreva, A. V. Anikina, A. B. Tarasov, E. A. Gudilin, A. V. Knotko, V. V. Volkov, K. A. Dembo, and Y. D. Tretyakov, *Dokl. Chem.* **410**, 165 (2006).
- <sup>17</sup>A. Grigorieva, Ph.D. thesis, M. V. Lomonosov Moscow State University, Moscow, 2009.
- <sup>18</sup>V. Petkov, P. Zavalij, S. Lutta, M. Whittingham, V. Parvanov, and S. Shastri, *Phys. Rev. B* **69**, 085410 (2004).
- <sup>19</sup>G. S. Zakharova, V. L. Volkov, V. V. Ivanovskaya, and A. L. Ivanovskii, *Russ. Chem. Rev.* **74**, 587 (2005).
- <sup>20</sup>S. V. Demishev, A. V. Semeno, H. Ohta, S. Okubo, I. E. Tarasenko, T. V. Ishchenko, N. A. Samarin, and N. E. Sluchanko, *Phys. Solid State* **49**, 1295 (2007).
- <sup>21</sup>N. Mott, *Metal Insulator Transitions* (Taylor and Francis, London, 1974).
- <sup>22</sup>S. Vonsovskii, *Magnetism* (Wiley, New York, 1979), p. 714.
- <sup>23</sup>Y. Nagaoka, *Phys. Rev.* **147**, 392 (1966).